Electron. Mater. Lett., Vol. 12, No. 6 (2016), pp. 761-767
DOI: 10.1007/s13391-016-6080-7

Fabrication of $Cu_2Zn(Sn,Si)S_4$ Thin Films Using a Two-Step Method for Solar Cell Applications

Jiaxiong Xu,* Yaqun Liu, and Yuanzheng Yang

School of Materials and Energy, Guangdong University of Technology, Guangzhou 510006, China

(received date: 17 March 2016 / accepted date: 23 August 2016 / published date: 10 November 2016)

To explore Cu_2ZnSnS_4-based materials for solar cell applications, for the first time, $Cu_2Zn(Sn,Si)S_4$ thin films were fabricated using a two-step method that consists of sputtering and post-sulfurization. The films were characterized and then incorporated into solar cells. X-ray diffraction and Raman spectroscopy revealed the formation of $Cu_2Zn(Sn,Si)S_4$ structure with traces of a secondary phase after sulfurization treatments. The degree of sulfurization was enhanced as the temperature was increased. In addition, these techniques revealed that there was no silicon or silicide phase present. The Si/Sn atomic ratio was 0.04-0.10. The thin films exhibited Cu-poor and Zn-rich characteristics and high absorption coefficients. The direct optical band gap of the thin films ranged between 1.42 and 1.52 eV. Heterojunction solar cells (glass/Mo/$Cu_2Zn(Sn,Si)S_4$/CdS/i-ZnO/ZnO:Al/Al) were fabricated and exhibited the highest conversion efficiency of 0.427%. This study showed the feasibilities of fabricating $Cu_2Zn(Sn,Si)S_4$ thin films by a two-step method and using $Cu_2Zn(Sn,Si)S_4$ thin films as an absorber layer within a solar cell.

Keywords: $Cu_2Zn(Sn,Si)S_4$, magnetron sputtering, sulfurization, thin films, solar cells

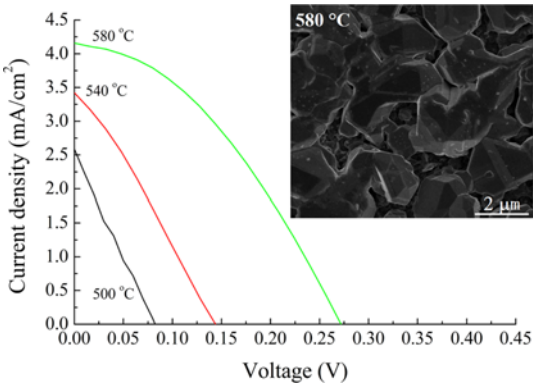

1. INTRODUCTION

Cu_2ZnSnS_4 thin films show potential as the next generation of absorber materials for solar cell applications.[1-3] They have absorption coefficients above 1×10^4 cm^{-1} in the visible region,[4-7] have a band gap that is suitable for single-junction solar cells (~1.5 eV),[1,5,8] show *p*-type conductivity, and are environmentally friendly.

Recent attention has focused on the semiconducting properties of $Cu_2Zn(Sn,Si)S_4$, which are similar to those of Cu_2ZnSnS_4.[9-11] For Cu_2ZnSnS_4, Sn loss occurs at high temperature owing to the volatility of SnS.[12,13] $Cu_2Zn(Sn,Si)S_4$ is formed by the partial substitution of Sn in Cu_2ZnSnS_4 with Si. This substitution is expected to inhibit Sn loss. To date, only single crystals of $Cu_2Zn(Sn,Si)S_4$ or $Cu_2ZnSiSe_4$ have been investigated.[9-11,14] The effect of substituting Sn with Si has also been studied.[11] Although the structure and properties of $Cu_2Zn(Sn,Si)S_4$ single crystals have been investigated, this material will be incorporated into solar cells as a thin film. To the best of our knowledge, the $Cu_2Zn(Sn,Si)S_4$ thin films have not been reported. Therefore, an understanding of the structure, properties, and fabrication methods of $Cu_2Zn(Sn,Si)S_4$ thin films and solar cells is critical.

In this work, we report a two-step method for the fabrication of $Cu_2Zn(Sn,Si)S_4$ thin films on soda-lime glass substrates. This involved the deposition of a Zn/Sn/Si/Cu stacked precursor followed by sulfurization treatment. Sulfurization treatment converted the stacked precursor into the desired $Cu_2Zn(Sn,Si)S_4$ structure. The structural, compositional, morphological, and optical properties of the thin

*Corresponding author: xujiaxiong@gdut.edu.cn

films were examined after sulfurization treatment at different temperatures. $Cu_2Zn(Sn,Si)S_4$ thin films were then incorporated as an absorber layer in solar cells.

2. EXPERIMENTAL PROCEDURE

Soda-lime glass was used as a substrate (2 cm × 1 cm × 1 mm). The glass substrates were cleaned using a standard process and then loaded into a magnetron sputtering chamber. The source materials used for deposition were Zn, Sn, Si, and Cu targets. The base and working pressures were 5×10^{-4} Pa and 0.5 Pa, respectively. During deposition, pure argon was introduced into the chamber at a flow rate of 20 mL/min. Zn, Sn, Si, and Cu were successively sputtered onto the glass substrates to form the Zn/Sn/Si/Cu stacked precursors. Zn and Cu were the bottom and top layers, respectively. Zn and Cu were sputtered using direct-current mode, and Sn and Si were deposited using radio frequency sputtering. The sputtering parameters for each layer are listed in Table 1.

After sputtering, the precursors were transferred into a tubular furnace for sulfurization treatment. Sulfur powder (99.95%, 1 g) was used as a source material. The sulfur powder and precursors were placed in a capped quartz boat positioned in the center of the tubular furnace. A N_2+S atmosphere was used for sulfurization with a N_2 flow rate of 250 mL/min. The furnace temperature as a function of time is shown in Fig. 1. The sulfurization treatment was performed in two steps: we first preheated the samples to 150 °C, and then heated them to the target temperature (500 °C, 540 °C, and 580 °C) for 30 min. The samples were then allowed to cool to ambient temperature in the tubular furnace.

Table 1. The sputtering parameters for Zn/Sn/Si/Cu stacked precursors.

Target	Sputtering power (W)	Sputtering time (s)
Zn	300	16
Sn	50	1140
Si	100	120
Cu	40	270

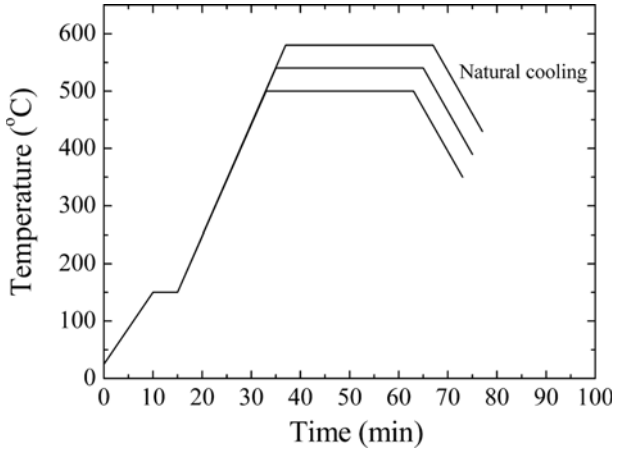

Fig. 1. Schematic of the temperature during sulfurization treatments.

The $Cu_2Zn(Sn,Si)S_4$ heterojunction solar cells had a structure consisting of glass/Mo (1 μm)/Cu_2Zn $(Sn,Si)S_4$/CdS (50 nm)/i-ZnO (50 nm)/ZnO:Al (800 nm)/Al (500 nm). A back contact Mo thin film was sputtered on the glass substrate. The $Cu_2Zn(Sn,Si)S_4$ absorber layer was then deposited on the Mo layer using the two-step method described previously. A CdS buffer layer was fabricated using chemical bath deposition followed by i-ZnO and ZnO:Al window layers that were deposited by magnetron sputtering. Finally, the Al front contact was sputtered in a finger pattern via mask.

The structural properties of the $Cu_2Zn(Sn,Si)S_4$ thin films were characterized using x-ray diffraction (XRD) (Rigaku D/MAX-Ultima IV, Cu-kα radiation, λ = 0.154 nm) and Raman spectroscopy (HORIBA Jobin Yvon, LabRAM HR800, λ = 633 nm). Field emission scanning electron microscopy (FESEM) (Hitachi SU8010) was used to observe the surface and cross-sectional morphologies of the $Cu_2Zn(Sn,Si)S_4$ thin films. The optical properties of the $Cu_2Zn(Sn,Si)S_4$ thin films were examined using an ultraviolet-visible spectrophotometer (Pgeneral, T6).

The elemental compositions of the $Cu_2Zn(Sn,Si)S_4$ thin films were measured using energy dispersive spectrometer (EDS). The substrate of the measured $Cu_2Zn(Sn,Si)S_4$ thin films was Mo foil because the Si in the soda-lime glass substrate would contribute to the measured results of the film's composition. The sputtering and sulfurization conditions used to fabricate the $Cu_2Zn(Sn,Si)S_4$ thin films on the Mo foil were identical to those used with the soda-lime glass substrates.

The photovoltaic performance of the $Cu_2Zn(Sn,Si)S_4$ thin film solar cells under simulated AM1.5 illumination was measured using a solar simulator and a digital source meter (Keithley 2400).

3. RESULTS AND DISCUSSION

XRD spectra of the thin films that were sulfurized at different temperatures are shown in Fig. 2. The thin film that was sulfurized at 500 °C exhibited peak characteristics of (112), (220), and (312) planes, which were typically observed in $Cu_2Zn(Sn,Si)S_4$.[10,11] When the sulfurization temperature was increased to 540 °C, an additional weak peak was identified at approximately 33 °, which was attributed to the (200) plane of $Cu_2Zn(Sn,Si)S_4$. The XRD spectrum of the thin film sulfurized at 580 °C contained a new peak characteristic of the (101) plane. All $Cu_2Zn(Sn,Si)S_4$ thin films had polycrystalline structures. The preferred orientation of the $Cu_2Zn(Sn,Si)S_4$ thin films was along the

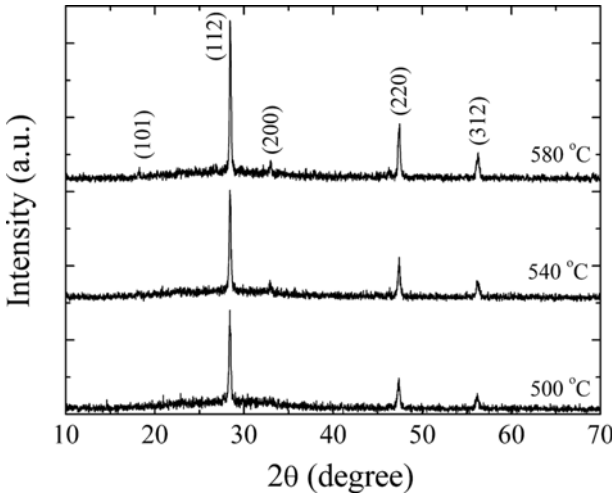

Fig. 2. The XRD spectra of $Cu_2Zn(Sn,Si)S_4$ thin films sulfurized at different temperatures.

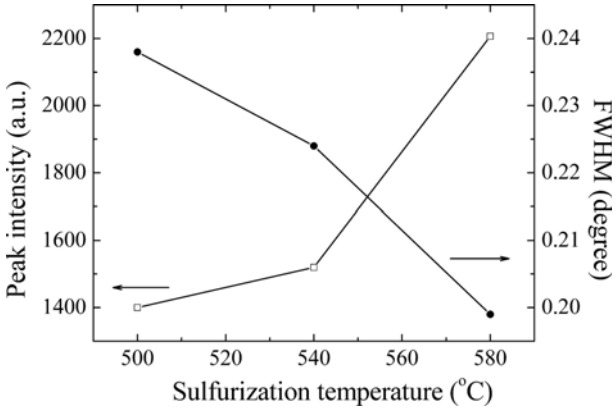

Fig. 3. The changes of intensity and FWHM of the preferred (112) peak with sulfurization temperature.

(112) plane, which was consistent with the reports of Cu_2ZnSnS_4 thin films[15-18] and $Cu_2Zn(Sn,Si)S_4$ single crystals.[10,11] XRD peak characteristics of silicon or silicides were not present in any of the XRD spectra.

The intensity and full width at half maximum (FWHM) of the peaks that correspond to the preferred (112) plane at different sulfurization temperatures are shown in Fig. 3. The peak intensity increased consistently with increasing sulfurization temperature, while the FWHM decreased. The peak intensity of the thin film sulfurized at 580 °C was 1.47 times that of the thin film sulfurized at 500 °C. The position of the (112) peak did not change with the sulfurization temperature, which indicated that the lattice constant of the $Cu_2Zn(Sn,Si)S_4$ thin films was independent of that temperature. The grain size (D) of a $Cu_2Zn(Sn,Si)S_4$ thin film is calculated using the Debye-Scherrer equation:

$$D = \frac{0.89\lambda}{\beta\cos\theta},$$

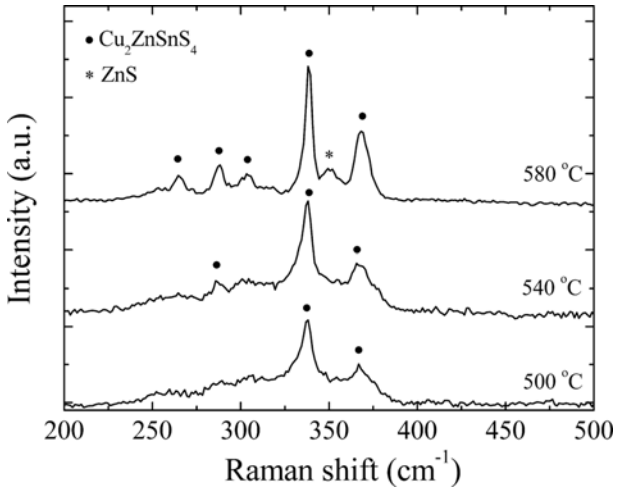

Fig. 4. The Raman spectra of $Cu_2Zn(Sn,Si)S_4$ thin films sulfurized at different temperatures.

where λ, β, and θ are the wavelength of Cu-kα radiation, the FWHM of the (112) peak, and the diffraction angle of the (112) peak, respectively. The values of D for the thin films that were sulfurized at 500 °C, 540 °C, and 580 °C were 34.0 nm, 36.2 nm, and 40.7 nm, respectively. These results revealed that the crystallinity of the thin films was enhanced as the sulfurization temperature increased, which was in agreement with literature reports for Cu_2ZnSnS_4.[5,19] The higher energies associated with higher temperatures enhanced the degree of sulfurization reaction, which resulted in increased crystallinity within the thin films.

As the XRD peaks (Fig. 2) may have originated from secondary phases of $Cu_2Zn(Sn,Si)S_4$, we used Raman scattering measurements to further characterize the phase structure of the thin films (Fig. 4). The Raman peaks observed in the spectra of the thin films (264 cm^{-1}, 288 cm^{-1}, 302 cm^{-1}, 338 cm^{-1}, and 367 cm^{-1}) had been previously assigned to the Cu_2ZnSnS_4 structure,[20] which indicated that the Cu_2ZnSnS_4 phase had formed in all of the thin films. The strongest peak located at 338 cm^{-1} was attributed to the A_1 mode of Cu_2ZnSnS_4, which was consistent with Cu_2ZnSnS_4 thin films.[21-23] Peak characteristics of silicon and related silicides were not detected in the Raman scattering spectra. The thin film that was sulfurized at 580 °C contained a secondary phase as evidenced by a peak characteristic of ZnS. Therefore, the phase structure of this thin film consisted of $Cu_2Zn(Sn,Si)S_4$ with traces of a secondary ZnS phase, which may have resulted from the decomposition of $Cu_2Zn(Sn,Si)S_4$ at the high sulfurization temperature used. As the sulfurization temperature increased, the Raman peak characteristics of Cu_2ZnSnS_4 increased and narrowed significantly, particularly the peaks located at 338 cm^{-1} and 367 cm^{-1}. This result indicated that the thin films were more crystalline, which was consistent with the XRD results.

Table 2. The compositional properties of the prepared thin films.

Sulfurization temperature (°C)	Cu (at.%)	Zn (at.%)	Sn (at.%)	Si (at.%)	S (at.%)	Cu/(Zn+Sn+Si)	Zn/(Sn+Si)	Si/Sn
500	15.95	19.92	9.08	0.89	54.16	0.53	2.00	0.10
540	16.54	21.41	8.79	0.32	52.94	0.54	2.35	0.04
580	17.09	19.90	9.86	0.67	52.48	0.56	1.89	0.07

The XRD and Raman results indicated that the stacked precursor layers (Zn/Sn/Si/Cu) interdiffused and reacted with sulfur during the sulfurization treatment, which led to the $Cu_2Zn(Sn,Si)S_4$ structure. The Si layer in the stacked precursor did not impede formation of the Cu_2ZnSnS_4 phase. The degrees of sulfurization and crystallinity of thin films depended on the sulfurization temperature. The sulfurization temperature was not increased further because of the potential for thermal instability of the soda-lime glass at higher temperatures. These results showed that $Cu_2Zn(Sn,Si)S_4$ thin films can be prepared successfully using the two-step method described.

The elemental composition of thin films fabricated on Mo foil substrates, including Cu, Zn, Sn, Si, and S, and the atomic ratios of Cu/(Zn+Sn+Si), Zn/(Sn+Si), and Si/Sn, are shown in Table 2. Mo was ignored during the EDS measurements. The S ratio in all of the thin films was close to the standard value of 50%. The ratios of Cu and Zn exhibited a degree of non-stoichiometry. All thin films were Cu-poor and Zn-rich, which was a requirement for solar cell applications using Cu_2ZnSnS_4.[24-26] However, the values of Cu/(Zn+Sn+Si) and Zn/(Sn+Si) deviated from the optimum values reported for Cu_2ZnSnS_4.[24-26] Therefore, the atomic percentages of Cu and Zn within the films need to be optimized in future work. The values of the Si/Sn ratio (0.04-0.10) indicated the substitution of Sn by Si.

Surface SEM images of the thin films sulfurized at 500 °C, 540 °C, and 580 °C are shown in Fig. 5. The surface of the thin film sulfurized at 500 °C (Fig. 5(a)) was inhomogeneous, and the grainy morphology was insignificant. Meanwhile, several voids appeared on the surface. The film that was sulfurized at 540 °C exhibited a slightly enlarged grain size. However, the distribution of the grains was still inhomogeneous. When the sulfurization temperature was increased to 580 °C, the grainy morphology was observed clearly; the grain size on the surface had increased significantly.

The cross-sectional SEM images of the $Cu_2Zn(Sn,Si)S_4$ thin films also exhibited grainy morphologies (Fig. 6). The grains enlarged with increasing sulfurization temperature. However, the voids also increased when the sulfurization temperature was increased to 580 °C, which was attributed to the decomposition of the $Cu_2Zn(Sn,Si)S_4$ structure. The thicknesses of the $Cu_2Zn(Sn,Si)S_4$ thin films, determined from the cross-sectional images, were 0.75 μm, 1 μm, and 1.25 μm when sulfurized at 500 °C, 540 °C, and 580 °C, respectively. The increased thickness suggested that the degree of sulfurization enhanced with increasing temperature.

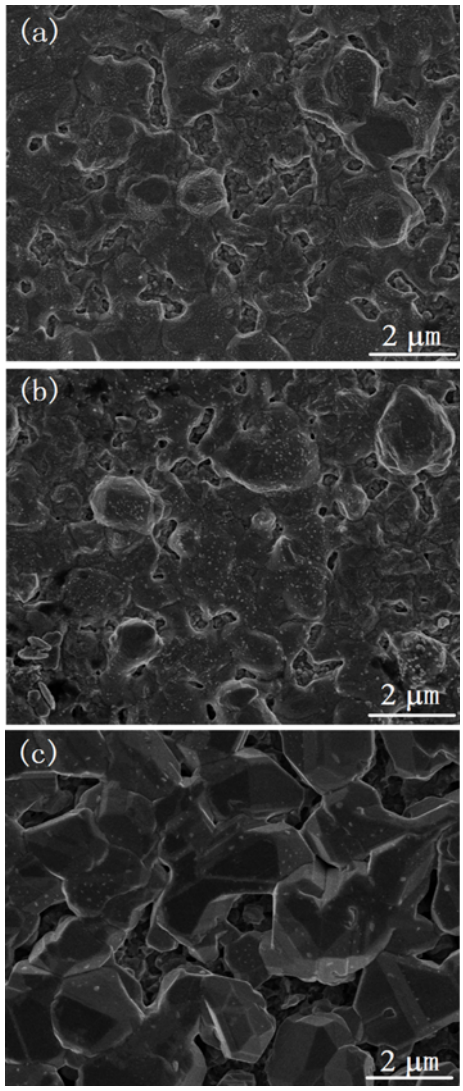

Fig. 5. The surface SEM images of $Cu_2Zn(Sn,Si)S_4$ thin films sulfurized at (a) 500 °C, (b) 540 °C, and (c) 580 C.

The transmittance of the thin films from 400 nm to 1000 nm is shown in Fig. 7. The transmittance in the visible region was lower than 8% for all films, revealing high absorption of $Cu_2Zn(Sn,Si)S_4$ thin films. The absorption coefficient (α) of a thin film is provided by the following equation:

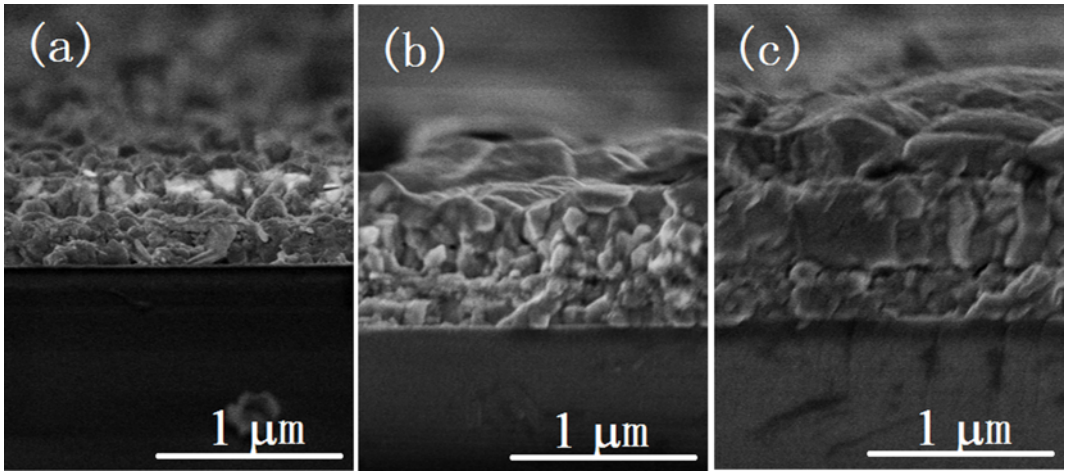

Fig. 6. The cross-sectional SEM images of $Cu_2Zn(Sn,Si)S_4$ thin films sulfurized at (a) 500 °C, (b) 540 °C, and (c) 580 °C.

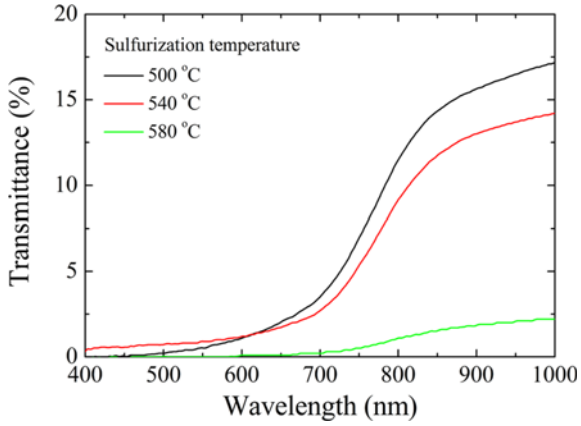

Fig. 7. The transmittance spectra of $Cu_2Zn(Sn,Si)S_4$ thin films.

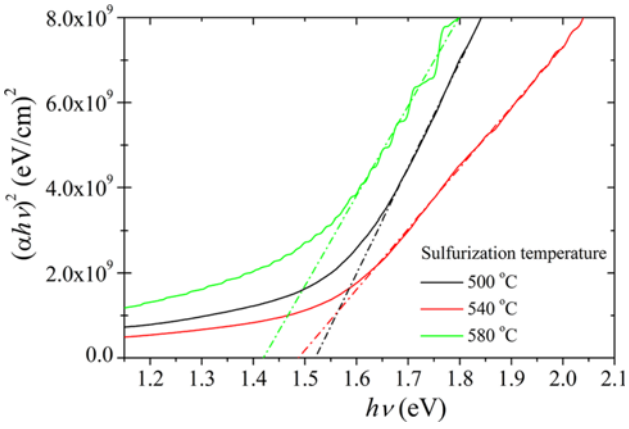

Fig. 8. The $(\alpha h\nu)^2$-$h\nu$ curves of $Cu_2Zn(Sn,Si)S_4$ thin films.

$$\alpha = \left(\frac{1}{d}\right)\ln\left(\frac{1}{T}\right),$$

where d and T are the thickness and transmittance of the thin film, respectively. The relationship between $(\alpha h\nu)^2$ and $h\nu$ for the thin films, where $h\nu$ is the photon energy, is shown in Fig. 8. A linear relationship existed in the high-energy region. The linear lines were extrapolated to the $h\nu$ axis (depicted by dashed lines) to give an estimation of the direct optical band gaps of the thin films (the intercept of the $h\nu$ axis). The direct optical band gaps for the thin films that were sulfurized at 500 °C, 540 °C, and 580 °C were 1.52 eV, 1.49 eV, and 1.42 eV, respectively. These values were similar to the reported band gaps for Cu_2ZnSnS_4 and $Cu_2Zn(Sn,Si)S_4$.[5,8,9] At lower sulfurization temperatures, the reduced grain size led to an increased optical band gap because of the quantum confinement effect. Above the optical band gap, the absorption coefficients of the $Cu_2Zn(Sn,Si)S_4$ thin films were on the order of 10^4 cm^{-1}, which was suitable for an absorber material in solar cells.

The current density-voltage (J-V) characteristics of the $Cu_2Zn(Sn,Si)S_4$ thin film solar cells under AM1.5 illumination are shown in Fig. 9. The open-circuit voltage (V_{oc}), short-

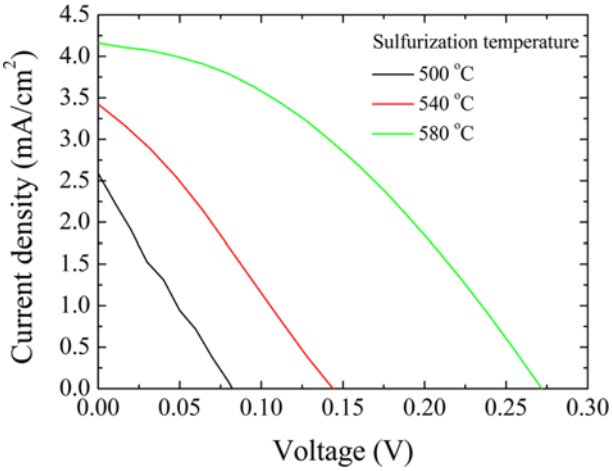

Fig. 9. The J-V characteristics of $Cu_2Zn(Sn,Si)S_4$ thin film solar cells when the absorbers sulfurized at different temperatures.

Table 3. The photovoltaic properties of $Cu_2Zn(Sn,Si)S_4$ thin film solar cells for different sulfurization temperatures.

Sulfurization temperature (°C)	V_{oc} (V)	J_{sc} (mA/cm^2)	*FF*	η (%)
500	0.08	2.58	0.25	0.051
540	0.14	3.42	0.29	0.139
580	0.27	4.16	0.38	0.427

circuit current density (J_{sc}), fill factor (*FF*), and conversion efficiency (η) of solar cells were obtained from the *J-V* curves and are given in Table 3. The photovoltaic properties of $Cu_2Zn(Sn,Si)S_4$ solar cells improved with the increasing sulfurization temperature, which was due to the enhanced crystallinity and thickness of $Cu_2Zn(Sn,Si)S_4$ absorber. However, the highest conversion efficiency of solar cells was only 0.427%, which was lower than that of Cu_2ZnSnS_4 thin film solar cells[1,2,4,16,18,25] and was limited by the low values of V_{oc}, J_{sc}, and *FF*. The reciprocal of the slope of the *J-V* curve at the short-circuit current point gave a shunt resistance of 336 Ω·cm^2 when $Cu_2Zn(Sn,Si)S_4$ sulfurized at 580 °C. The low values of the shunt resistance led to low conversion efficiency. The voids that were revealed from the cross-sectional SEM images may have produced parasitic current paths, which resulted in the reduction of the shunt resistance. Although the $Cu_2Zn(Sn,Si)S_4$ thin film solar cells exhibited inferior photovoltaic performances, this work showed that $Cu_2Zn(Sn,Si)S_4$ thin films can be successfully incorporated and used as an absorber layer within solar cells.

4. CONCLUSIONS

Zn/Sn/Si/Cu-layered stacks were sputtered onto soda-lime glass substrates as precursor films, which were then subjected to sulfurization. The successful fabrication of the $Cu_2Zn(Sn,Si)S_4$ thin films using a two-step method involving magnetron sputtering and post-sulfurization was confirmed using a combination of XRD, Raman spectroscopy, and SEM. The preferred orientation of the $Cu_2Zn(Sn,Si)S_4$ thin films was along the (112) plane. The XRD, Raman, and SEM results revealed that the degrees of sulfurization and crystallinity within the $Cu_2Zn(Sn,Si)S_4$ thin films were enhanced at higher sulfurization temperatures. The composition of thin films was Cu-poor and Zn-rich, with an atomic ratio of Si/Sn that varied from 0.04 to 0.10. The direct optical band gap ranged between 1.42 and 1.52 eV. Heterojunction solar cells were fabricated (glass/Mo/$Cu_2Zn(Sn,Si)S_4$/CdS/i-ZnO/ZnO:Al/Al) that exhibited the highest conversion efficiency of 0.427%. Further work is required to optimize the prepared conditions for improving the properties of the $Cu_2Zn(Sn,Si)S_4$ solar cells that incorporate these films.

ACKNOWLEDGEMENTS

This work was supported by National Natural Science Foundation of China (No. 61504029).

REFERENCES

1. T. Todorov, O. Gunawan, S. J. Chey, T. G. de Monsabert, A. Prabhakar, and D. B. Mitzi, *Thin Solid Films* **519**, 7378 (2011).
2. K. Ramasamy, M. A. Malik, and P. O'Brien, *Chem. Commun.* **48**, 5703 (2012).
3. A. V. Moholkar, S. S. Shinde, G. L. Agawane, S. H. Jo, K. Y. Rajpure, P. S. Patil, C. H. Bhosale, and J. H. Kim, *J. Alloys Compd.* **544**, 145 (2012).
4. K. Jimbo, R. Kimura, T. Kamimura, S. Yamada, W. S. Maw, H. Araki, K. Oishi, and H. Katagiri, *Thin Solid Films* **515**, 5997 (2007).
5. J. X. Xu, Z. M. Cao, Y. Z. Yang, and Z. W. Xie, *J. Renew. Sustain. Energy* **6**, 053110 (2014).
6. M. Xie, D. M. Zhuang, M. Zhao, B. J. Li, M. J. Cao, and J. Song, *Vacuum* **101**, 146 (2014).
7. J. Ge, W. L. Yu, H. Cao, J. C. Jiang, J. H. Ma, L. H. Yang, P. X. Yang, Z. G. Hu, and J. H. Chu, *Phys. Status Solidi A* **209**, 1493 (2012).
8. J. X. Xu, Z. M. Cao, and Y. Z. Yang, *Chalcogenide Lett.* **12**, 529 (2015).
9. M. Hamdi, A. Lafond, C. Guillot-Deudon, F. Hlel, M. Gargouri, and S. Jobic, *J. Solid State Chem.* **220**, 232 (2014).
10. M. Hamdi, B. Chrif, A. Lafond, B. Louati, C. Guillot-Deudon, and F. Hlel, *J. Alloys Compd.* **643**, 129 (2015).
11. M. Hamdi, B. Louati, A. Lafond, C. Guillot-Deudon, B. Chrif, K. Khirouni, M. Gargouri, S. Jobic, and F. Hlel, *J. Alloys Compd.* **620**, 434 (2015).
12. A. Redinger, D. M. Berg, P. J. Dale, and S. Siebentritt, *J. Am. Chem. Soc.* **133**, 3320 (2011).
13. A. Weber, R. Mainz, and H. W. Schock, *J. Appl. Phys.* **107**, 013516 (2010).
14. K. G. Lisunov, M. Guc, S. Levcenko, D. Dumcenco, Y. S. Huang, G. Gurieva, S. Schorr, and E. Arushanov, *J. Alloys Compd.* **580**, 481 (2013).
15. J. X. Xu, Y. Z. Yang, Z. M. Cao, and Z. W. Xie, *Optik* **127**, 1567 (2016).
16. Y. Z. Zhang, Q. Y. Ye, J. Liu, H. Chen, X. L. He, C. Liao, J. F. Han, H. Wang, J. Mei, and W. M. Lau, *RSC Adv.* **4**, 23666 (2014).
17. W. Daranfed, M. S. Aida, N. Attaf, J. Bougdira, and H. Rinnert, *J. Alloys Compd.* **542**, 22 (2012).
18. S. M. Pawara, A. I. Inamdara, B. S. Pawar, K. V. Gurav, S. W. Shin, X. Yanjun, S. S. Kolekar, J. H. Lee, J. H. Kim, and H. Im, *Mater. Lett.* **118**, 76 (2014).
19. H. Yoo, J. H. Kim, and L. X. Zhang, *Curr. Appl. Phys.* **12**, 1052 (2012).

20. P. A. Cormier and R. Snyders, *Acta. Mater.* **96**, 80 (2015).
21. O. Vigil-Galan, M. Espindola-Rodriguez, M. Courel, X. Fontane, D. Sylla, V. Izquierdo-Roca, A. Fairbrother, E. Saucedo, and A. Perez-Rodriguez, *Sol. Energ. Mat. Sol. C.* **117**, 246 (2013).
22. B. Pani and U. P. Singh, *J. Renew. Sustain. Energy* **5**, 053131 (2013).
23. K. J. Wang, B. Shin, K. B. Reuter, T. Todorov, D. B. Mitzi, and S. Guha, *Appl. Phys. Lett.* **98**, 051912 (2011).
24. Q. Guo, G. M. Ford, W. C. Yang, B. C. Walker, E. A. Stach, H. W. Hillhouse, and R. Agrawal, *J. Am. Chem. Soc.* **132**, 17384 (2010).
25. K. Tanaka, M. Oonuki, N. Moritake, and H. Uchiki, *Sol. Energ. Mat. Sol. C.* **93**, 583 (2009).
26. A. Nagoya, R. Asahi, R. Wahl, and G. Kresse, *Phys. Rev. B* **81**, 113202 (2010).